Functional plasticity of polarity proteins controls epithelial tissue architecture

Cornélia Biehler[1,2], Katheryn E. Rothenberg[3,4], Alexandra Jetté[1,2], Hélori-Mael Gaudé[1,2], Rodrigo Fernandez-Gonzalez[3,4,5,6], and Patrick Laprise[1,2*]

[1]Centre de Recherche sur le Cancer, Université Laval, and [2]axe oncologie du Centre de Recherche du Centre Hospitalier Universitaire de Québec-UL, 9 McMahon, Québec, QC, G1R 3S3, Canada. [3]Institute of Biomaterials and Biomedical Engineering, University of Toronto, Toronto, ON M5S 3G9, Canada. [4]Ted Rogers Centre for Heart Research, University of Toronto, Toronto, ON M5G 1M1, Canada. [5]Department of Cell and Systems Biology, University of Toronto, Toronto, ON M5S 3G5, Canada. [6]Developmental and Stem Cell Biology Program, The Hospital for Sick Children, Toronto, ON M5G 1X8, Canada.

[*]Author for correspondence: Patrick.Laprise@crchudequebec.ulaval.ca, Phone : (418) 525-4444 ext. 16959, Fax : (418) 691-5439

Key words: Yurt, Crumbs, aPKC, Pak1, Myosin II, epithelial morphogenesis, apical constriction, cellular tension.

Abstract

The *Drosophila* polarity protein Crumbs is essential for the establishment and growth of the apical domain in epithelial cells. Dynamic regulation of apical domain size is crucial for forming and maintaining complex epithelial structures such as tubes or acini. The protein Yurt limits the ability of Crumbs to promote apical membrane growth, thereby defining proper apical/basal membrane ratio that is essential for the functional architecture of epithelial cells. Here, we show that Yurt is not a general inhibitor of Crumbs, but rather hijacks Crumbs activity toward specific functions. In particular, Crumbs recruits Yurt to the apical domain to increase Myosin-dependent cortical tension while decreasing relative tissue viscosity. Yurt overexpression thus induces apical constriction in epithelial cells. The kinase aPKC phosphorylates Yurt, thereby dislodging the latter from the apical domain and releasing apical tension. In contrast, the kinase Pak1 promotes Yurt dephosphorylation through activation of the phosphatase PP2A. The Pak1–PP2A module thus opposes aPKC function and supports Yurt-induced apical constriction. Hence, the complex interplay between Yurt, aPKC, Pak1 and PP2A contributes to the functional plasticity of Crumbs. Overall, our data increase our understanding of how proteins sustaining epithelial cell polarization and Myosin-dependent cell contractility interact with one another to control epithelial tissue architecture.

Introduction

Simple epithelia form cohesive barriers owing to specialized adherens junctions. For instance, the cadherin–catenin complex, a major component of the *zonula adherens* (ZA), links cortical actin filaments of neighboring cells indirectly to ensure strong cell–cell adhesion (1). Association of the hexameric motor protein non-muscle myosin II (hereafter, myosin) with ZA-associated actin bundles ensures contractility (2). The ability of epithelial cells to support vectorial transport and secretion adjusts the biochemical environment on both sides of the epithelial layer. These unidirectional functions require the polarization of epithelial cells along the apical–basal axis (3). Reciprocal interactions between the epithelial polarity protein network and ZA components not only define the functional architecture of individual epithelial cells, but also shape epithelial tissues (4). A classic example is the formation of specialized epithelial structures, such as tubes or acini, resulting from concerted myosin-dependent apical constriction of a group of cells within epithelial sheets (5).

The apically localized protein Crumbs (Crb) acts as an apical determinant in *Drosophila* epithelia (4, 6-8). The cytoplasmic tail of Crb contains a PSD95/Dlg1/ZO-1 (PDZ)-domain binding motif (PBM), and a Four point one, Ezrin, Radixin, Moesin (FERM)-domain binding motif (FBM) (4, 8-10). The PBM recruits PDZ-containing proteins such as Stardust (Sdt), which cooperates with Crb in establishing the apical membrane and promoting its growth (8, 11, 12). The FBM interacts with several FERM domain proteins, including Yurt (Yrt) (13, 14). The latter is localized to the lateral membrane throughout embryogenesis, and supports the stability of this membrane domain during organogenesis (13, 15). During terminal differentiation of epithelial cells derived from the ectoderm, Yrt also occupies the apical membrane due to a direct interaction with Crb (13). The

apical recruitment of Yrt limits Crb-dependent apical membrane growth to establish a specific apical/basolateral membrane size ratio, which is crucial to defining the morphometric parameters of developing epithelial structures (13, 16). Crb displays cooperative functional interactions with atypical protein kinase C (aPKC) and its binding partner Partitioning defective protein 6 (Par-6) (4, 17-19). These latter apical proteins act downstream of the small GTPase Cdc42 to promote phospho-dependent inhibition of lateral polarity proteins such as Lethal (2) giant larvae [L(2)gl] and Yrt (3, 4, 20-23). In return, L(2)gl and Yrt repress aPKC function to prevent the spread of apical characteristics to the lateral domain (13, 15, 20-22, 24-27). Mutual antagonism between apical and lateral protein modules thus establishes a sharp boundary between their respective membrane domains (3, 22). Cdc42 also activates p21-activated kinase 1 (Pak1), which has substrates in common with aPKC in fly epithelial cells (28). However, it remains to be determined whether Pak1 targets the full complement of aPKC substrates, and whether phosphorylation by these kinases always has the same functional impact on target proteins and epithelial cell polarity. In particular, the functional relationship linking Pak1 and Yrt remains unexplored.

The mammalian Yrt orthologs EPB41L4B and EPB41L5 (also known as EHM2/LULU2 and YMO1/LULU, respectively) support cell migration and invasion, and EPB41L5 is also essential for the epithelial–mesenchymal transition (EMT) (29-37). Given that Crb and human CRUMBS3 (CRB3) both repress EMT (38, 39), these observations are consistent with the aforementioned concept that fly and mammalian Yrt proteins repress the Crb/CRB3-containing apical machinery (3, 13). However, recent findings have shown that depletion of Crb or Yrt causes similar phenotypes in pupal wing cells. Specifically, E-cadherin (E-cad) staining is fragmented, and F-Actin and Myosin distribution is altered in the absence of these proteins (40). This suggests that Yrt controls cell contractility – a premise that awaits formal demonstration. Consistent with this

model, it was shown that EPB41L4B and EPB41L5 promote MYOSIN-dependent apical constriction (41-43). Similar to EPB41L4B and EPB41L5, *Drosophila* Crb organizes the actomyosin cytoskeleton at cell–cell contacts, thereby supporting ZA integrity and tissue morphogenesis (44-46). Crb fulfils this function in ectodermal cells in part through the apical recruitment of the Guanine exchange factor (GEF) Cysts (Cyst), which activates the Rho1–Rho kinase (Rok)–Myosin pathway (46-48). In contrast, other studies have reported that Crb stabilizes adherens junctions by repressing Myosin activity (49). Moreover, Crb was shown to reduce the membrane residence time of Rok, thereby preventing the formation of a supracellular actomyosin cable in cells expressing high Crb levels at the salivary gland placode boundary where Crb distribution is anisotropic (50, 51). These conflicting observations show that the functional relationship linking Crb and Myosin is complex, and likely context-dependent. Whether, and how, Yrt modulates the multifaceted function of Crb in regulating cytoskeletal dynamics remains as an outstanding puzzle. Here, we show that Crb recruits Yrt to the apical membrane to induce Myosin-dependent apical tension in *Drosophila* epithelial cells. This association and the ensuing increased Myosin activity is repressed by aPKC-dependent phosphorylation of Yrt. In contrast to aPKC, Pak1 maintains the pool of unphosphorylated Yrt via activation of Protein phosphatase 2A (PP2A), thereby supporting Yrt-dependent cortical tension.

Results

Yrt increases Myosin-dependent cortical tension and promotes apical constriction

It was previously shown that loss of Yrt expression increases cell diameter in pupal tissues (40), thus suggesting that Yrt may promote actomyosin-based contraction to define cell width. To test this hypothesis directly, we measured retraction velocity after laser ablation of cell borders in the *Drosophila* embryonic epidermis, which reflects Myosin-dependent cortical tension (52). Knockdown of *yrt* expression decreased retraction velocity (Fig. 1A, B), whereas Yrt overexpression had the opposite effect (Fig. 1C, D). We quantified changes to the material properties of the apical cell surface using a Kelvin-Voigt model to measure the relaxation times of laser ablation experiments, proportional to the viscosity-to-elasticity ratio (53). We found that *yrt* knockdown and Yrt overexpression had opposite effects, with *yrt* knockdown causing a relative increase in viscosity (longer relaxation times, Fig. 1E) and Yrt overexpression leading to a local tissue fluidization (shorter relaxation times, Fig. 1F). Moreover, mosaic expression of FLAG-Yrt (mRFP-positive cells) in the ovarian follicular epithelium induced apical constriction (Fig. 1G, H). FLAG-Yrt expression also resulted in apical enrichment of Spaghetti squash (Sqh), the *Drosophila* Myosin regulatory light chain, knockdown of which suppressed Yrt-induced apical constriction (Fig. 1I–L). Taken together, these results establish that Yrt promotes Myosin-based changes in cell mechanics to support cortical tension and apical constriction.

aPKC counteracts Yrt-induced apical constriction by preventing the Crb-dependent apical recruitment of Yrt

aPKC phosphorylates Yrt on evolutionarily conserved residues (20). This prevents Yrt oligomerization, thereby antagonizing its ability to support lateral membrane stability and to

restrict apical membrane growth (54). Expression of membrane-targeted aPKC (aPKC^{CAAX}) suppressed FLAG-Yrt-induced apical constriction (Fig. 2A–C, H), showing that aPKC has a broad impact on Yrt function and also alters its ability to promote Myosin activity. However, aPKC^{CAAX} had no effect on apical constriction induced by FLAG-Yrt^{5A} in which the amino acids targeted by aPKC were replaced by non-phosphorylatable alanine residues [(20); Fig. 2D, E, H]. In addition, mutation of the aPKC phosphorylation sites into aspartic acids to generate the phosphomimetic Yrt mutant protein FLAG-Yrt^{5D} (20) abolished the ability of Yrt to induce apical constriction (Fig. 2F, I). Similarly, a FLAG-Yrt mutant protein unable to oligomerize [FLAG-Yrt^{FWA}; (54)] failed to sustain apical constriction (Fig. 2G, I). These results argue strongly that aPKC targets Yrt directly to inhibit its ability to support apical constriction.

To gain further insights on how aPKC impacts on Yrt function in the follicular epithelium, we analyzed Yrt subcellular localization upon modulation of aPKC activity. We observed apical accumulation of Yrt in wild-type cells treated with a chemical inhibitor of aPKC or in *aPKC* knockdown cells (Fig. 2J, K). These results show that aPKC normally acts to restrict Yrt apical localization, which depends on Crb in the embryonic epidermis and in pupal photoreceptor cells (13). This is also the case in adult follicular epithelial cells, as Yrt failed to accumulate apically in *crb* mutant cells treated with the aPKC inhibitor (Fig. 2L; *crb* mutant cells are positively labeled with GFP). Similarly, Yrt was absent from the apical membrane upon inhibition of aPKC in cells exclusively expressing a mutant Crb protein containing an amino acid substitution inactivating its FBM [Crb^{Y10A}; (Fig. 2O); (9)], which precludes the direct association of Yrt and Crb proteins (13). This suggests that aPKC precludes cortical tension by repressing the Yrt–Crb association, and thus argues that Crb plays a pivotal role in Yrt-dependent apical constriction. Accordingly, FLAG-Yrt^{5A} triggered apical constriction in wild-type cells, whereas it was unable to induce this phenotype in

Crb-depleted cells or cells expressing Crb^{Y10A} (Fig. 2M, N, P, Q). Together, these results demonstrate that the Crb–Yrt complex promotes cortical tension and apical constriction. Our data also establish that aPKC prevents excessive tension at the apical domain by phosphorylating Yrt and preventing its recruitment by Crb.

Pak1 and PP2A decrease Yrt phosphorylation and are required for Yrt-induced apical constriction

It was recently shown that aPKC and Pak1 share common phosphorylation targets, namely the polarity proteins L(2)gl, Bazooka (40), Par6, and Crb (28). It was also proposed that aPKC and Pak1 act redundantly on these substrates (28). However, it remains to be determined whether Pak1 impacts the function of other aPKC substrates such as Yrt. In addition, it is unclear if aPKC and Pak1 function is fully redundant in epithelial cells, or whether these kinases also have specific roles. To shed light on these issues, we first analyzed the impact of Pak1 inhibition on Yrt localization in the follicular epithelium. The Pak1 inhibitor IPA-III strongly reduced membrane localization of Yrt (Fig. 3A). Overexpression of Par6 together with $aPKC^{CAAX}$, which accumulated ectopically at the lateral membrane, mimicked this phenotype (Fig. 3B). Overexpression of Par6 and $aPKC^{CAAX}$ is also associated with an upward shift in the gel migration profile of Yrt (Fig. 3C). This resulted from increased Yrt phosphorylation, as treatment of samples with the λ Phosphatase prior to electrophoresis abolished the impact of $aPKC^{CAAX}$ on Yrt gel mobility [Fig. 3C; (20)]. These results raise the intriguing possibility that Pak1 inhibition results in increased phosphorylation of Yrt on aPKC target sites, thereby preventing Yrt association with the membrane. In accordance with this hypothesis, overexpression of membrane-targeted Pak1 [$Pak1^{Myr}$; (55)] decreased Yrt phosphorylation levels (Fig. 3C). Given that Pak1 is a kinase, these

observations are counterintuitive. However, it has been shown that Pak1 can activate the phosphatase PP2A (56), thus raising the possibility that the latter targets Yrt downstream of Pak1. Accordingly, Yrt phosphorylation levels were increased strongly in *PP2A-A* mutant embryos, or in wild-type embryos treated with the PP2A inhibitor Cantharidin (Fig. 3D, E). Strikingly, inhibition of PP2A suppressed the impact of Pak1^{Myr} expression on Yrt phosphorylation (Fig. 3F), arguing that PP2A acts downstream of Pak1.

We next tested the functional impact of Pak1- and PP2A-dependent modulation of Yrt phosphorylation. Chemical inhibition of Pak1 or PP2A, or knockdown of their expression suppressed apical constriction induced by FLAG-Yrt (Fig. 4A–H). Of note, FLAG-Yrt^{5A} maintained its ability to induce apical constriction in the presence of Cantharidin, or when PP2A was depleted (Fig. 4E–H), further supporting the idea that PP2A acts on aPKC target sites to sustain Yrt function. Altogether, these data suggest that Pak1 acts upstream of PP2A, which antagonizes aPKC function by dephosphorylating Yrt, thereby allowing the latter to induce apical tension.

Discussion

Myosin-mediated cell contractility impacts a broad range of cellular processes driving tissue morphogenesis, including apical constriction, convergent extension, and ZA establishment and maintenance (57, 58). Our data establish that Yrt increases Myosin-dependent cortical tension in embryonic and adult tissues, thereby providing further insights into how Yrt contributes to organize epithelial tissue architecture. In addition, our analysis suggested that Yrt decreases tissue viscosity, thereby highlighting a putative role of Yrt in Actin organization. Similarly, a recent study showed that loss of Yrt expression increases cell diameter in pupal wing cells (40), thus suggesting that Yrt controls the actomyosin network throughout the fly life cycle. This function is evolutionarily conserved, as the mammalian Yrt proteins EPB41L4B and EPB41L5 impact actomyosin organization and stimulate apical constriction (41-43). Regulation of actomyosin contractility by Yrt likely impacts ZA stability, as suggested by the fragmented distribution of ZA components in Yrt-depleted cells [(40); Biehler and Laprise, unpublished results]. This is in line with the fact that Yrt-induced apical constriction depends on Crb, which is also required for organization of junctional Myosin assembly and ZA stability (8, 44, 46). Activation of the Rho1–Rok pathway contributes to these functions of Crb (46). However, we found that decreasing Rho1 or Rok activity do not significantly reduce Yrt-induced apical constriction (Biehler and Laprise, unpublished results). This implies that Crb acts through multiple pathways to fine-tune actomyosin contractility. We are currently exploring the molecular mechanisms by which the Crb–Yrt complex controls Myosin activity and increases cortical tension.

Our findings showing that Crb and Yrt cooperate in promoting cortical tension may seem at odds with previous studies demonstrating that Yrt inhibits the ability of Crb to promote apical membrane

growth (13, 15). We propose that Yrt is not a general inhibitor of Crb function, but rather acts downstream of Crb to specifically control actomyosin contractility at the expense of other Crb-dependent roles such as apical membrane growth. It is possible that the recruitment of Yrt causes steric hindrance on the short cytoplasmic tail of Crb, thereby preventing the binding of Crb effectors mediating apical membrane growth. Our current model is that the numerous functions of Crb are specified by the presence or absence, and the identity of, the FERM domain protein within distinct Crb complexes. This paradigm is in accordance with our data establishing the role of the Crb–Yrt complex in apical tension as well as previous findings showing that Crb controls cell growth through recruitment of the FERM domain protein Expanded (Ex) (59, 60). Moreover, it has been shown that Moesin (Moe; a FERM family member) acts downstream of Crb to fulfil multiple roles (45, 49, 61-65), some of which counteract Yrt function. For instance, it was shown that loss of Moe decreases cell diameter in wing epithelial cells (40), suggesting that Moe reduces cortical tension in these cells. Thus, fine regulation of the incorporation of different FERM-domain proteins within distinct Crb complexes most likely dictates the biological output downstream of Crb. This ordered equilibrium may explain the functional plasticity of Crb, which can both increase or decrease Myosin-dependent contractility to accommodate dynamic regulation of epithelial cell polarity, cell–cell adhesion, and tissue morphogenesis (45, 46, 49-51, 63). Further studies are required to test the intriguing possibility that this concept is generalizable to other receptors/FERM-domain protein signaling modules.

Our discoveries indicate that aPKC prevents the Crb–Yrt association through direct phosphorylation of Yrt. Thereby, aPKC excludes Yrt from the apical membrane and represses Yrt-induced apical constriction. aPKC also inhibits the ability of Yrt to restrict Crb-dependent apical membrane growth (20, 54). This is consistent with the aforementioned model, and with previous

reports documenting functional cooperation between aPKC and Crb in establishing the apical domain (4, 22, 66, 67). We have shown that phosphorylation of Yrt on aPKC target sites prevents Yrt self-association, and that oligomerization-defective Yrt mutant proteins are unable to bind Crb (54). Together, these studies establish that the phospho-dependent repression of Yrt oligomerization is a key mechanism by which aPKC controls apical–basal polarity, cortical tension, and epithelial cell architecture. Our data also show that ectopic localization of aPKC to the lateral domain dislodges Yrt from the membrane, indicating that aPKC controls both Crb-dependent and Crb-independent membrane localization of Yrt. One possibility is that phosphorylation of Yrt by aPKC generates electrostatic repulsion with negatively charged membrane phospholipids, as described for other aPKC substrates (68). Tight regulation of the phosphorylation of Yrt on aPKC target sites is thus crucial for the integrity of both apical and lateral domains.

Cdc42 is a key regulator of epithelial cell polarity acting upstream of aPKC and Pak1 (28, 69). These kinases share common substrates and have redundant functions in apical–basal polarity regulation (28). However, the Yrt sequence does not contain a Pak1 consensus motif. Moreover, we found that expression of membrane-targeted Pak1 reduces Yrt phosphorylation levels, whereas membrane-bound aPKC has the opposite effect. This argues that Yrt is not a direct substrate of Pak1, and that this kinase does not phosphorylate the full complement of aPKC substrates within the polarity protein network. Our results also indicate that Pak1 and aPKC have opposite effects on Yrt membrane localization, as inhibition of Pak1 or aPKC activation displaces Yrt from the membrane. Finally, while Pak1 is required for Yrt-induced apical constriction, aPKC inhibits this function of Yrt. In the light of all of this evidence, we propose that Pak1 promotes the dephosphorylation of aPKC target sites on Yrt to support its functions. We provide evidence that Pak1 acts through phosphatase PP2A to achieve this function in polarized epithelial cells. PP2A

thus has a broad role in cell polarity, as it opposes aPKC and Par-1 signaling to control the polarized architecture of neuroblasts and photoreceptor cells (70-72). In these cell types, PP2A targets Par6 and/or Baz. This implies that Pak1 may also decrease the phosphorylation level of Baz and/or Par6 in epithelial cells, although the kinase domain of Pak1 can phosphorylate Baz and Par6 *in vitro* (28). At this point, a cell type-specific or context-dependent regulation of Baz and Par-6 by Pak1 cannot be ruled out. Alternatively, it is possible that Pak1 can both increase or decrease the phosphorylation of specific polarity proteins in regulatory feedback loops, thereby ensuring the delicate equilibrium required for epithelial tissue homeostasis. Combining our data with the work of Aguilar-Aragon et al. (28) suggests that activation of aPKC and Pak1 downstream of Cdc42 has redundant activity on a subset of polarity proteins [e.g. Par6, L(2)gl, Baz], while having opposite effects on Yrt and apical tension. Identification of the molecular mechanisms selecting the engagement of aPKC or Pak1 downstream of Cdc42 remains an outstanding puzzle, solving of which will provide crucial insights into the understanding of epithelial cell polarity, cortical tension, and tissue morphogenesis.

Overall, our work reveals a novel mechanism regulating cortical tension at the apical domain, which plays a crucial role in developing and adult epithelia. We also refine our understanding of the functional relationship linking Crb and Yrt by establishing that the latter contributes to the plasticity of Crb function rather than acting as an obligatory inhibitor of the apical protein machinery. We also highlight that the roles of aPKC and Pak1 are not fully redundant in epithelial cells, and that these kinases have opposite effects on cortical tension. We also provide evidence that Pak1 can decrease protein phosphorylation in epithelial cells through PP2A, thereby consolidating the broad role played by this phosphatase in cell polarity. These findings may serve

as basis to elaborate molecular strategies to target EPB41L4B and EPB41L5 in cancer cells, thereby preventing invasion and metastasis (29-35).

Materials and methods

Drosophila genetics

The UAS-GAL4 system was employed to drive the expression of transgenes (73). Mosaic analysis in the follicular epithelium was performed using the Flippase recognition target (FRT)/Flippase (FLP) system in which the FLP recombinase was under the control of a heat shock promoter (*hsFLP*) (74, 75). Newly hatched females were heat-shocked for 3 h at 37°C on two consecutive days. Ovaries were dissected and processed 48 h after the second heat shock. Table 1 and 2 depict the stock list and the complete genotype of flies used in this study, respectively.

Laser ablation for measurement of mechanical properties

Stage 14 embryos were dechorionated for 2 minutes in 50% bleach, washed with water, and glued on a coverslip using heptane glue (76). Ablations were induced using a pulsed Micropoint N_2 laser (Andor) tuned to 365 nm on a Revolution XD spinning disk confocal microscope. The laser produces 120 μJ pulses at durations of 2-6 ns each. For ablation of cell junctions, 10 consecutive laser pulses were delivered to a single spot along a cell interface. Images were acquired every 3 s before and after ablation of a single interface using a 60x oil immersion lens (Olympus, NA 1.35). The positions of the tricellular vertices connected by the ablated interface were manually tracked prior to and for 1 min following ablation using the image analysis platform SIESTA (77, 78). To measure retraction velocity, the change in distance between the tricellular vertices was measured comparing images acquired immediately before and after ablation and divided by the time elapsed between the two images. To quantify the viscoelastic properties of the tissue, we modelled the laser ablation results as the damped recoil of an elastic fibre, using a Kelvin-Voigt mechanical-equivalent circuit (53). Briefly, the Kelvin-Voigt circuit models cell interfaces as a spring

(elasticity) and a dashpot (viscosity) configured in parallel. As a result, the distance between the ends of the interface when tension is released can be quantified as:

$$L(t) = D\left(1 - e^{-\frac{t}{\tau}}\right)$$

where $L(t)$ is the distance between the tricellular vertices at the end of the severed interface at time t after ablation, D is the asymptotic value of the distance between the tricellular junctions, and the relaxation time τ:

$$\tau = \frac{\mu}{E}$$

is the ratio of the viscosity (μ) to the elasticity (E) of the tissue. Statistical differences between groups were measured using the nonparametric Mann-Whitney U test.

Immunofluorescence

Dissected ovaries were fixed for 15 min in 4% paraformaldehyde or heat fixed (aPKC, Yrt, and Arm stainings) as previously described (20). Fixed ovaries were blocked for 1 h in NGT (2% normal goat serum, 0.3% Triton X-100 in PBS). Ovaries were incubated with the following primary antibodies overnight at 4°C: mouse anti-Dlg1 [4F3, Developmental Studies Hybridoma Bank at the University of Iowa (DSHB)], 1:25 dilution; rabbit anti-Yurt, 1:1000 (79); guinea-pig anti-Yurt (13), 1:250; mouse anti-GFP (Roche, Sigma Aldrich), 1:200; mouse anti-Fas3 (7G10, DSHB), 1:10; rabbit anti-RFP (600-401-379, Rockland), 1:400; mouse anti-Armadillo (N27A1, DSHB), 1:100; rabbit anti-aPKC (C-20, Santa Cruz Biotechnology), 1:200. Ovaries were then washed three times in PBT (0.3% Triton X-100 in PBS) before and after incubation with secondary antibodies (1:400 in NGT, 1 h at room temperature), which were conjugated to Cy3 (Jackson ImmunoResearch Laboratories) or Alexa Fluor 488 (Molecular Probes). Ovarioles were

mechanically separated and mounted in Vectashield mounting medium (Vector Labs), and imaged with a LSM700 confocal (63× Apochromat lens with a numerical aperture of 1.40). Images were uniformly processed with ImageJ (National Institutes of Health).

Phosphatase assays

Dechorionated embryos were homogenized in ice-cold lysis buffer (1% Triton X-100, 50 mM TRIS-HCl pH 7.5, 5% glycerol, 150 mM NaCl, 1 mM PMSF, 0.5 μg/mL aprotinin, 0.7 μg/mL pepstatin, and 0.5 μg/mL leupeptin). Lysates were cleared by centrifugation at 4°C, and 400 units of λ Phosphatase (New England Biolabs) was added to 30 μg of proteins extracted from embryos. The volume of the reaction mix was completed to 30 μl with the MetalloPhosphatase buffer (New England Biolabs) containing 1 mM of $MnCl_2$ prior to a 30-min incubation at 30°C. The reaction was stopped by addition of Laemmli's buffer.

Western blotting

Dechorionated embryos were homogenized in ice-cold lysis buffer (1% Triton X-100, 50 mM TRIS HCl pH 7.5, 5% glycerol, 100 mM NaCl, 50 mM NaF, 5 mM EDTA pH 8, 40 mM β-glycerophosphate, 1 mM PMSF, 0.5 μg/mL aprotinin, 0.7 μg/mL pepstatin, 0.5 μg/mL leupeptin and 0.1 mM orthovanadate) and processed for SDS-PAGE and western blotting as previously described (80). Primary antibodies used: Rabbit anti-Yrt (79), 1:10000; mouse anti-β–Tubulin (E7, DSHB), 1:2000; rabbit anti-aPKC (C-20, Santa Cruz Biotechnology), 1:2000; rabbit anti-PP2A-A (72), 1:10000; mouse anti-Actin (NB-100-74340, Novus Biologicals), 1:2000. HRP-conjugated secondary antibodies were from GE Healthcare and used at a 1:2000 dilution.

Chemical treatment of embryos

Dechorionated embryos were incubated under agitation for 1 h at room temperature in a 0.9% NaCl solution supplemented with 100 μM of Cantharidin under an octane phase (1:1). Embryos were then washed three times in PBT.

Chemical treatment of ovaries

Dissected ovaries were treated for 2 h with inhibitors of aPKC (CRT-006-68-54, Bio-Techn Sales Corporation, 10 μM) or Pak1 (IPA-III, Millipore Sigma, 10 μM for immunolocalization experiments and 50 μM for apical constriction assays) as described (81).

Measurements of apical domain size and quantification of fluorescence intensity

Stage 3−6 follicles were imaged, and the apical diameter or fluorescence intensity of genetically modified cells (positively labeled with mRFP or GFP) was measured using ImageJ (National Institutes of Health). Control cells facing labeled cells on the opposite side of the follicle were used as control. Results are expressed as the ratio between measurements in labeled cells and control cells. A minimum of 20 follicles were analyzed in each condition. Statistical differences between groups were determined using one-way ANOVA (apical domain size) or Student's t-test (fluorescence intensity).

Figure legends

Fig 1. Yrt increases apical tension

A. Epidermal cells in stage 14 *Drosophila* embryos expressing E-cad::GFP and shRNA against *mCherry* or *yrt* before (cyan in merge) and after (magenta in merge) laser ablation of a cell-cell interface (white arrowheads). Scale bars, 3 µm. **B**. Retraction velocity after laser ablation in embryos expressing shRNA against *mCherry* (n = 17 junctions) or *yrt* (n = 17). **C**. Epidermal cells in stage 14 *Drosophila* embryos expressing E-cad::GFP and no perturbation of Yrt expression (left panel) or overexpression of FLAG-Yrt (right panel) before (cyan in merge) and after (magenta in merge) ablation of a cell-cell interface (white arrowheads). Scale bars, 3 µm. **D**. Retraction velocity after laser ablation in embryos with wild-type Yrt expression (n = 13 junctions) or overexpressing FLAG-Yrt (n = 15). **E, F**. Relaxation time after laser ablation in embryos expressing shRNA against *mCherry* (n = 17 junctions) or *yrt* (n = 17) (**E**), or in wild-type (n = 13) and FLAG-Yrt expressing embryos (n = 15) (**F**). In **B–F**, error bars indicate the standard deviation (s.d.), and black lines denote the mean. * $P \leq 0.05$, ** $P \leq 0.01$, *** $P \leq 0.001$ (Mann-Whitney test). **G**. Mosaic expression of mRFP and LacZ (control; left panels), or membrane-targeted RFP (mRFP) and FLAG-Yrt (right panels) in the follicular epithelium. Immunostaining of mRFP highlights cells expressing the transgenes, whereas immunolabeling of endogenous Discs large 1 (Dlg1; green) marks the lateral membrane of all epithelial cells. **H**. Quantification of apical domain width of cells expressing the transgenes listed in G. Results are expressed as the ratio between the width of cells expressing the transgenes and the width of wild-type cells in the same follicle (see methods). **I**. Mosaic expression of FLAG-Yrt in follicular epithelial cells constitutively expression Sqh::GFP, which was visualized by immunofluorescence. FLAG-Yrt-expressing cells (right panels) are labeled with mRFP, which was expressed with LacZ in control clones (left panels). **J**.

Quantification of the fluorescence intensity of apical Sqh::GFP in cells expressing the exogenous proteins described in I. Results were calculated as a ratio between FLAG-Yrt-expressing cells and control cells in the same follicle. **K**. Mosaic expression of a shRNA targeting *sqh* (left panels), of FLAG-Yrt (center panels), or expression of both sh-*sqh* and FLAG-Yrt (right panels). mRFP was co-expressed with these constructs, and was used to label positive cells. **L**. Quantification of the apical diameter of cells expressing the transgenes indicated in K. Results are expressed as a ratio to the width of control cells. In H, J, and L, error bars indicate s.d.; bold black lines denote the mean; $n \geq 20$; **** $P \leq 0.0001$ (one-way ANOVA for H, L; Student's t-test for J). Scale bars represent 5 μm.

Fig 2. aPKC antagonizes the ability of the Crb-Yrt complex to induce apical constriction. A-G. Clonal expression of the indicated proteins in the follicular epithelium. Clones were positively labeled with mRFP. Yurt staining was used to identify positive cells in C and E. **H, I**. Quantification of the apical diameter of cells expressing the transgenes indicated in A–E (H) or F, G (I). Results are expressed as a ratio to the width of control cells. **J**. Panels depict immunofluorescence of Yrt (green) and Fasciclin 3 (Fas3; magenta) in the follicular epithelium treated for 2 h with the vehicle DMSO or the aPKC inhibitor CRT-006-68-54 (aPKC inh.). **K**. *aPKC* knockdown cells (mRFP positive) were immunostained for Yrt. **L**. crb^{11A22} homozygous mutant clones were produced in adult *crb*/+ female flies (mutant clones are GFP positive). Dissected ovaries were incubated with the vehicle DMSO or CRT-006-68-54 (aPKC inh.) prior to fixation and Yrt immunostaining. **M**. FLAG-Yrt^{5A} was specifically expressed in *crb* mutant cell clones (right panels). Mosaic expression of FLAG-Yrt^{5A} in wild-type cells or *crb* mutant clones were used as controls (middle and left panels, respectively). Clones were labeled with GFP (left panels) or by Yrt immunostaining

(middle and right panels). Dlg1 staining was used to label the lateral membrane. **N**. Quantification of the apical domain width of cells expressing the transgenes listed in M. Results are expressed as the ratio between the width of cells expressing the transgenes and the width of wild-type cells in the same follicle. **O**. Immunostaining of Yrt and Dlg1 in follicular epithelial cells expressing FLAG-Yrt and exogenous wild-type Crb (left panels), or FLAG-Yrt together with Crb^{Y10A} (right panels) specifically in *crb* null cell clones. **Q**. Quantification of the apical domain width of cells expressing the transgenes listed in P. Results are expressed as the ratio between the width of cells expressing the transgenes and the width of wild-type cells in the same follicle. In H, I, N, and Q error bars indicate s.d.; bold black lines denote the mean; $n \geq 20$; **** $P \leq 0.0001$ (one-way ANOVA). All scale bars represent 5 μm.

Fig 3. Pak1 and PP2A control the phosphorylation level of Yrt

A. Wild-type follicles were incubated with the vehicle DMSO or the Pak1 inhibitor IPA-III (Pak1 inh) prior to fixation and immunostaining with anti-Yrt and anti-Fas3 antibodies. **B**. Yrt and aPKC (upper panels), or Fas3 and aPKC (lower panels) immunostainings in control follicular epithelial cells or clones of cells expressing $aPKC^{CAAX}$ together with Par6. Scale bars represent 5 μm. **C**. Control embryos, embryos overexpressing Par-6 and $aPKC^{CAAX}$, or embryos expressing $Pak1^{Myr}$ were homogenized. Samples were incubated or not with the λ phosphatase and processed for SDS-PAGE. Western blotting using anti-Yrt antibodies showed the migration profile of phosphorylated (^{p}Yrt) or unphosphorylated Yrt, whereas β-Tubulin (βTub) was used as loading control. **D**. Western blots showing the migration profile of Yrt (^{p}Yrt stands for phosphorylated Yrt) extracted from wild-type (WT) or *PP2A-A* mutant embryos, and the levels of PP2A-A. Actin was used as loading control. **E**. Wild-type embryos were treated or not with the PP2A inhibitor Cantharidin

(PP2A inh.), homogenized, and processed for SDS-PAGE. Western blotting using control samples shows the phosphorylation levels of Yrt (^{P}Yrt), whereas samples incubated with λ phosphatase (λ PPase) prior to gel electrophoresis show unphosphorylated Yrt. β-Tubulin (βTub) was used as loading control. **F**. Embryos overexpressing Pak1^{Myr} were treated or not with PP2A inhibitor and homogenized. Western blotting using anti-Yrt antibodies showed the migration profile of phosphorylated (^{P}Yrt) or unphosphorylated Yrt. λ Phosphatase was used as a positive control of Yrt dephosphorylation, and β-Tubulin (βTub) was used as loading control.

Fig 4. Pak1 and PP2A are essential for Yrt-induced apical constriction

A. Follicles clonally overexpressing FLAG-Yrt were incubated with the vehicle DMSO or the Pak1 inhibitor (IPA-III; Pak1 inh) prior to fixation and immunostaining with antibodies directed against Yrt and Dlg1. **B**. Quantification of the apical diameter of cells expressing transgenes indicated in A. Results are expressed as the ratio between the width of cells expressing the transgenes and the width of wild-type cells in the same follicle. **C**. Immunostaining of Dlg1 in follicles displaying mosaic expression of a shRNA targeting *Pak1*, FLAG-Yrt, or both transgenes. Clones were labeled with mRFP. **D**. Quantification of the diameter of cells expressing the exogenous proteins described in C. Results were calculated as a ratio between FLAG-Yrt-expressing cells and control cells. **E**. Follicles containing cell clones expressing FLAG-Yrt or FLAG-Yrt^{5A} (mRFP positive cells) were incubated or not with the PP2A inhibitor Cantharidin prior to immunostaining with indicated antibodies. **F**. Quantification of the apical diameter of cells expressing transgenes indicated in E. Results are expressed as the ratio between the width of cells expressing the transgenes and the width of wild-type cells in the same follicle. **G**. Panels depict follicular epithelium displaying mosaic knockdown of *PP2A-A* (left panels), mosaic expression of FLAG-Yrt (middle panels), or a

combination of both (right panels). Immunostaining of mRFP or Yrt highlights cells expressing the transgenes, whereas immunolabeling of endogenous Dlg1 shows the lateral domain of epithelial cells. **H**. Quantification of the apical diameter of cells expressing transgenes indicated in G. Results are expressed as the ratio between the width of cells expressing the transgenes and the width of wild-type cells in the same follicle. B, D, F, H. Error bars indicate s.d.; bold black lines denote the mean; $n \geq 16$; * $P \leq 0.05$, **** $P \leq 0.0001$ (one-way ANOVA). All scale bars represent 5 μm.

Acknowledgments

The authors would like to acknowledge A. Wodarz, S. Campuzano, T. Harris, E. Knust, D. St-Johston, Y. Bellaiche, N. Perrimon, the Bloomington *Drosophila* Stock Center, the *Drosophila* Genomics Resource Center, and the Developmental Studies Hybridoma Bank for reagents. Flybase was used as an important database for this work. We also thank C. Gamblin for critical reading of the manuscript. This work was supported by operating grants from the Canadian Institute of Health Research (CIHR) to P.L. (MOP-142236) and R.F.G (MOP-156279). C.B. is supported by a scholarship from FRQ-S, and K. R. is a postdoctoral CIHR grantee.

Author contributions

C.B. and P.L. conceived the project in collaboration with K.R. and R.F.-G. C.B., K.R., A.J., and H.-M.G. performed experiments, prepared reagents, and contributed to data analysis. C.B. and P.L. interpreted most results. P.L. wrote the manuscript, which was proofread by co-authors. Finally, C.B., K.R., and P.L. assembled the figures. All authors read and approved the final manuscript.

Competing interests

The authors declare no competing financial interests.

REFERENCES

1. T. J. Harris, U. Tepass, Adherens junctions: from molecules to morphogenesis. *Nature reviews. Molecular cell biology* **11**, 502-514 (2010).

2. R. M. Mege, N. Ishiyama, Integration of Cadherin Adhesion and Cytoskeleton at Adherens Junctions. *Cold Spring Harbor perspectives in biology* **9** (2017).

3. P. Laprise, U. Tepass, Novel insights into epithelial polarity proteins in Drosophila. *Trends Cell Biol* S0962-8924(11)00039-0 [pii]

10.1016/j.tcb.2011.03.005 (2011).

4. U. Tepass, The Apical Polarity Protein Network in Drosophila Epithelial Cells: Regulation of Polarity, Junctions, Morphogenesis, Cell Growth, and Survival. *Annu Rev Cell Dev Biol* 10.1146/annurev-cellbio-092910-154033 (2012).

5. A. C. Martin, B. Goldstein, Apical constriction: themes and variations on a cellular mechanism driving morphogenesis. *Development* **141**, 1987-1998 (2014).

6. A. Wodarz, U. Hinz, M. Engelbert, E. Knust, Expression of crumbs confers apical character on plasma membrane domains of ectodermal epithelia of Drosophila. *Cell* **82**, 67-76 (1995).

7. U. Tepass, C. Theres, E. Knust, crumbs encodes an EGF-like protein expressed on apical membranes of Drosophila epithelial cells and required for organization of epithelia. *Cell* **61**, 787-799 (1990).

8. S. M. Pocha, E. Knust, Complexities of Crumbs function and regulation in tissue morphogenesis. *Current biology : CB* **23**, R289-293 (2013).

9. A. Klebes, E. Knust, A conserved motif in Crumbs is required for E-cadherin localisation and zonula adherens formation in Drosophila. *Current biology : CB* **10**, 76-85 (2000).

10. S. Klose, D. Flores-Benitez, F. Riedel, E. Knust, Fosmid-based structure-function analysis reveals functionally distinct domains in the cytoplasmic domain of Drosophila crumbs. *G3 (Bethesda)* **3**, 153-165 (2013).

11. U. Tepass, E. Knust, Crumbs and stardust act in a genetic pathway that controls the organization of epithelia in Drosophila melanogaster. *Developmental biology* **159**, 311-326 (1993).

12. A. Bachmann, M. Schneider, E. Theilenberg, F. Grawe, E. Knust, Drosophila Stardust is a partner of Crumbs in the control of epithelial cell polarity. *Nature* **414**, 638-643 (2001).

13. P. Laprise *et al.*, The FERM protein Yurt is a negative regulatory component of the Crumbs complex that controls epithelial polarity and apical membrane size. *Developmental cell* **11**, 363-374 (2006).

14. U. Tepass, FERM proteins in animal morphogenesis. *Curr Opin Genet Dev* **19**, 357-367 (2009).

15. P. Laprise *et al.*, Yurt, Coracle, Neurexin IV and the Na(+),K(+)-ATPase form a novel group of epithelial polarity proteins. *Nature* **459**, 1141-1145 (2009).

16. P. Laprise *et al.*, Epithelial polarity proteins regulate Drosophila tracheal tube size in parallel to the luminal matrix pathway. *Current biology : CB* **20**, 55-61 (2010).

17. O. Kempkens *et al.*, Computer modelling in combination with in vitro studies reveals similar binding affinities of Drosophila Crumbs for the PDZ domains of Stardust and DmPar-6. *Eur J Cell Biol* **85**, 753-767 (2006).

18. D. S. Whitney *et al.*, Binding of Crumbs to the Par-6 CRIB-PDZ Module Is Regulated by Cdc42. *Biochemistry* **55**, 1455-1461 (2016).

19. E. Morais-de-Sa, V. Mirouse, D. St Johnston, aPKC phosphorylation of Bazooka defines the apical/lateral border in Drosophila epithelial cells. *Cell* **141**, 509-523 (2010).

20. C. L. Gamblin, E. J. Hardy, F. J. Chartier, N. Bisson, P. Laprise, A bidirectional antagonism between aPKC and Yurt regulates epithelial cell polarity. *The Journal of cell biology* **204**, 487-495 (2014).

21. A. Hutterer, J. Betschinger, M. Petronczki, J. A. Knoblich, Sequential roles of Cdc42, Par-6, aPKC, and Lgl in the establishment of epithelial polarity during Drosophila embryogenesis. *Developmental cell* **6**, 845-854 (2004).

22. G. C. Fletcher, E. P. Lucas, R. Brain, A. Tournier, B. J. Thompson, Positive feedback and mutual antagonism combine to polarize Crumbs in the Drosophila follicle cell epithelium. *Current biology : CB* **22**, 1116-1122 (2012).

23. F. C. Peterson, R. R. Penkert, B. F. Volkman, K. E. Prehoda, Cdc42 regulates the Par-6 PDZ domain through an allosteric CRIB-PDZ transition. *Mol Cell* **13**, 665-676 (2004).

24. M. L. Drummond, K. E. Prehoda, Molecular Control of Atypical Protein Kinase C: Tipping the Balance between Self-Renewal and Differentiation. *J Mol Biol* **428**, 1455-1464 (2016).

25. G. Tanentzapf, U. Tepass, Interactions between the crumbs, lethal giant larvae and bazooka pathways in epithelial polarization. *Nature cell biology* **5**, 46-52 (2003).

26. D. Bilder, M. Schober, N. Perrimon, Integrated activity of PDZ protein complexes regulates epithelial polarity. *Nature cell biology* **5**, 53-58 (2003).

27. T. Yamanaka *et al.*, Lgl mediates apical domain disassembly by suppressing the PAR-3-aPKC-PAR-6 complex to orient apical membrane polarity. *Journal of cell science* **119**, 2107-2118 (2006).

28. M. Aguilar-Aragon *et al.*, Pak1 Kinase Maintains Apical Membrane Identity in Epithelia. *Cell Rep* **22**, 1639-1646 (2018).

29. H. Handa, A. Hashimoto, S. Hashimoto, H. Sabe, Arf6 and its ZEB1-EPB41L5 mesenchymal axis are required for both mesenchymal- and amoeboid-type invasion of cancer cells. *Small GTPases* 10.1080/21541248.2016.1249043, 0 (2016).

30. A. Hashimoto *et al.*, ZEB1 induces EPB41L5 in the cancer mesenchymal program that drives ARF6-based invasion, metastasis and drug resistance. *Oncogenesis* **5**, e259 (2016).

31. M. H. Jeong *et al.*, EPB41L5 Mediates TGFbeta-Induced Metastasis of Gastric Cancer. *Clin Cancer Res* **25**, 3617-3629 (2019).

32. Y. Otsuka *et al.*, High expression of EPB41L5, an integral component of the Arf6-driven mesenchymal program, correlates with poor prognosis of squamous cell carcinoma of the tongue. *Cell Commun Signal* **14**, 28 (2016).

33. J. Saller *et al.*, EPB41L5 is Associated With the Metastatic Potential of Low-grade Pancreatic Neuroendocrine Tumors. *Cancer Genomics Proteomics* **16**, 309-318 (2019).

34. J. Wang *et al.*, Increased expression of the metastasis-associated gene Ehm2 in prostate cancer. *Prostate* **66**, 1641-1652 (2006).

35. H. Yu, L. Ye, R. E. Mansel, Y. Zhang, W. G. Jiang, Clinical implications of the influence of Ehm2 on the aggressiveness of breast cancer cells through regulation of matrix metalloproteinase-9 expression. *Mol Cancer Res* **8**, 1501-1512 (2010).

36. M. Hirano, S. Hashimoto, S. Yonemura, H. Sabe, S. Aizawa, EPB41L5 functions to post-transcriptionally regulate cadherin and integrin during epithelial-mesenchymal transition. *The Journal of cell biology* **182**, 1217-1230 (2008).

37. J. D. Lee, N. F. Silva-Gagliardi, U. Tepass, C. J. McGlade, K. V. Anderson, The FERM protein Epb4.1l5 is required for organization of the neural plate and for the epithelial-mesenchymal transition at the primitive streak of the mouse embryo. *Development* **134**, 2007-2016 (2007).

38. K. Campbell, G. Whissell, X. Franch-Marro, E. Batlle, J. Casanova, Specific GATA factors act as conserved inducers of an endodermal-EMT. *Developmental cell* **21**, 1051-1061 (2011).

39. E. L. Whiteman, C. J. Liu, E. R. Fearon, B. Margolis, The transcription factor snail represses Crumbs3 expression and disrupts apico-basal polarity complexes. *Oncogene* **27**, 3875-3879 (2008).

40. P. Salis *et al.*, Crumbs, Moesin and Yurt regulate junctional stability and dynamics for a proper morphogenesis of the Drosophila pupal wing epithelium. *Sci Rep* **7**, 16778 (2017).

41. H. Nakajima, T. Tanoue, Epithelial cell shape is regulated by Lulu proteins via myosin-II. *Journal of cell science* **123**, 555-566 (2010).

42. H. Nakajima, T. Tanoue, The circumferential actomyosin belt in epithelial cells is regulated by the Lulu2-p114RhoGEF system. *Small GTPases* **3**, 91-96 (2012).

43. H. Nakajima, T. Tanoue, Lulu2 regulates the circumferential actomyosin tensile system in epithelial cells through p114RhoGEF. *The Journal of cell biology* **195**, 245-261 (2011).

44. U. Tepass, Crumbs, a component of the apical membrane, is required for zonula adherens formation in primary epithelia of Drosophila. *Developmental biology* **177**, 217-225 (1996).

45. A. Letizia, S. Sotillos, S. Campuzano, M. Llimargas, Regulated Crb accumulation controls apical constriction and invagination in Drosophila tracheal cells. *Journal of cell science* **124**, 240-251 (2011).

46. J. T. Silver *et al.*, Apical polarity proteins recruit the RhoGEF Cysts to promote junctional myosin assembly. *The Journal of cell biology* **218**, 3397-3414 (2019).

47. G. M. Rubin *et al.*, Comparative genomics of the eukaryotes. *Science* **287**, 2204-2215 (2000).

48. T. R. Arnold, R. E. Stephenson, A. L. Miller, Rho GTPases and actomyosin: Partners in regulating epithelial cell-cell junction structure and function. *Experimental cell research* **358**, 20-30 (2017).

49. D. Flores-Benitez, E. Knust, Crumbs is an essential regulator of cytoskeletal dynamics and cell-cell adhesion during dorsal closure in Drosophila. *Elife* **4** (2015).

50. K. Roper, Anisotropy of Crumbs and aPKC drives myosin cable assembly during tube formation. *Developmental cell* **23**, 939-953 (2012).

51. C. Sidor, T. J. Stevens, L. Jin, J. Boulanger, K. Roper, Rho-Kinase Planar Polarization at Tissue Boundaries Depends on Phospho-regulation of Membrane Residence Time. *Developmental cell* **52**, 364-378 e367 (2020).

52. M. S. Hutson *et al.*, Forces for morphogenesis investigated with laser microsurgery and quantitative modeling. *Science* **300**, 145-149 (2003).

53. R. Fernandez-Gonzalez, M. Simoes Sde, J. C. Roper, S. Eaton, J. A. Zallen, Myosin II dynamics are regulated by tension in intercalating cells. *Developmental cell* **17**, 736-743 (2009).

54. C. L. Gamblin *et al.*, Oligomerization of the FERM-FA protein Yurt controls epithelial cell polarity. *The Journal of cell biology* 10.1083/jcb.201803099 (2018).

55. N. K. Noren, B. P. Liu, K. Burridge, B. Kreft, p120 catenin regulates the actin cytoskeleton via Rho family GTPases. *J Cell Biol* **150**, 567-580 (2000).

56. K. Staser *et al.*, A Pak1-PP2A-ERM signaling axis mediates F-actin rearrangement and degranulation in mast cells. *Exp Hematol* **41**, 56-66 e52 (2013).

57. K. Z. Perez-Vale, M. Peifer, Orchestrating morphogenesis: building the body plan by cell shape changes and movements. *Development* **147** (2020).

58. H. Miao, J. T. Blankenship, The pulse of morphogenesis: actomyosin dynamics and regulation in epithelia. *Development* **147** (2020).

59. C. Ling *et al.*, The apical transmembrane protein Crumbs functions as a tumor suppressor that regulates Hippo signaling by binding to Expanded. *Proceedings of the National Academy of Sciences of the United States of America* **107**, 10532-10537 (2010).

60. B. S. Robinson, J. Huang, Y. Hong, K. H. Moberg, Crumbs regulates Salvador/Warts/Hippo signaling in Drosophila via the FERM-domain protein Expanded. *Current biology : CB* **20**, 582-590 (2010).

61. E. Medina *et al.*, Crumbs interacts with moesin and beta(Heavy)-spectrin in the apical membrane skeleton of Drosophila. *The Journal of cell biology* **158**, 941-951 (2002).

62. B. E. Kerman, A. M. Cheshire, M. M. Myat, D. J. Andrew, Ribbon modulates apical membrane during tube elongation through Crumbs and Moesin. *Developmental biology* **320**, 278-288 (2008).

63. A. T. Bajur, K. V. Iyer, E. Knust, Cytocortex-dependent dynamics of Drosophila Crumbs controls junctional stability and tension during germ band retraction. *Journal of cell science* **132** (2019).

64. F. Hochapfel *et al.*, Distinct functions of Crumbs regulating slit diaphragms and endocytosis in Drosophila nephrocytes. *Cell Mol Life Sci* **74**, 4573-4586 (2017).

65. K. M. Sherrard, R. G. Fehon, The transmembrane protein Crumbs displays complex dynamics during follicular morphogenesis and is regulated competitively by Moesin and aPKC. *Development* **142**, 1869-1878 (2015).

66. S. Sotillos, M. T. Diaz-Meco, E. Caminero, J. Moscat, S. Campuzano, DaPKC-dependent phosphorylation of Crumbs is required for epithelial cell polarity in Drosophila. *The Journal of cell biology* **166**, 549-557 (2004).

67. R. F. Walther, F. Pichaud, Crumbs/DaPKC-dependent apical exclusion of Bazooka promotes photoreceptor polarity remodeling. *Current biology : CB* **20**, 1065-1074 (2010).

68. M. J. Bailey, K. E. Prehoda, Establishment of Par-Polarized Cortical Domains via Phosphoregulated Membrane Motifs. *Developmental cell* **35**, 199-210 (2015).

69. F. Pichaud, R. F. Walther, F. Nunes de Almeida, Regulation of Cdc42 and its effectors in epithelial morphogenesis. *Journal of cell science* **132** (2019).

70. H. Ogawa, N. Ohta, W. Moon, F. Matsuzaki, Protein phosphatase 2A negatively regulates aPKC signaling by modulating phosphorylation of Par-6 in Drosophila neuroblast asymmetric divisions. *Journal of cell science* **122**, 3242-3249 (2009).

71. S. C. Nam, B. Mukhopadhyay, K. W. Choi, Antagonistic functions of Par-1 kinase and protein phosphatase 2A are required for localization of Bazooka and photoreceptor morphogenesis in Drosophila. *Developmental biology* **306**, 624-635 (2007).

72. M. P. Krahn, D. Egger-Adam, A. Wodarz, PP2A antagonizes phosphorylation of Bazooka by PAR-1 to control apical-basal polarity in dividing embryonic neuroblasts. *Developmental cell* **16**, 901-908 (2009).

73. A. H. Brand, A. S. Manoukian, N. Perrimon, Ectopic expression in Drosophila. *Methods Cell Biol* **44**, 635-654 (1994).

74. K. G. Golic, S. Lindquist, The FLP recombinase of yeast catalyzes site-specific recombination in the Drosophila genome. *Cell* **59**, 499-509 (1989).

75. T. B. Chou, N. Perrimon, The autosomal FLP-DFS technique for generating germline mosaics in Drosophila melanogaster. *Genetics* **144**, 1673-1679 (1996).

76. G. Scepanovic, A. Florea, R. Fernandez-Gonzalez, Multiscale In Vivo Imaging of Collective Cell Migration in Drosophila Embryos. *Methods Mol Biol* **2179**, 199-224 (2021).

77. R. Fernandez-Gonzalez, J. A. Zallen, Oscillatory behaviors and hierarchical assembly of contractile structures in intercalating cells. *Phys Biol* **8**, 045005 (2011).

78. C. Y. Leung, R. Fernandez-Gonzalez, Quantitative image analysis of cell behavior and molecular dynamics during tissue morphogenesis. *Methods Mol Biol* **1189**, 99-113 (2015).

79. C. Biehler *et al.*, Girdin is a component of the lateral polarity protein network restricting cell dissemination. *PLoS Genet* **16**, e1008674 (2020).

80. P. Laprise *et al.*, Phosphatidylinositol 3-kinase controls human intestinal epithelial cell differentiation by promoting adherens junction assembly and p38 MAPK activation. *The Journal of biological chemistry* **277**, 8226-8234 (2002).

81. F. J. Chartier, E. J. Hardy, P. Laprise, Crumbs limits oxidase-dependent signaling to maintain epithelial integrity and prevent photoreceptor cell death. *The Journal of cell biology* **198**, 991-998 (2012).

82. J. Huang, W. Zhou, W. Dong, A. M. Watson, Y. Hong, From the Cover: Directed, efficient, and versatile modifications of the Drosophila genome by genomic engineering.

Proceedings of the National Academy of Sciences of the United States of America **106**, 8284-8289 (2009).

83. A. Royou, C. Field, J. C. Sisson, W. Sullivan, R. Karess, Reassessing the role and dynamics of nonmuscle myosin II during furrow formation in early Drosophila embryos. *Molecular biology of the cell* **15**, 838-850 (2004).

84. M. V. Staller *et al.*, Depleting gene activities in early Drosophila embryos with the "maternal-Gal4-shRNA" system. *Genetics* **193**, 51-61 (2013).

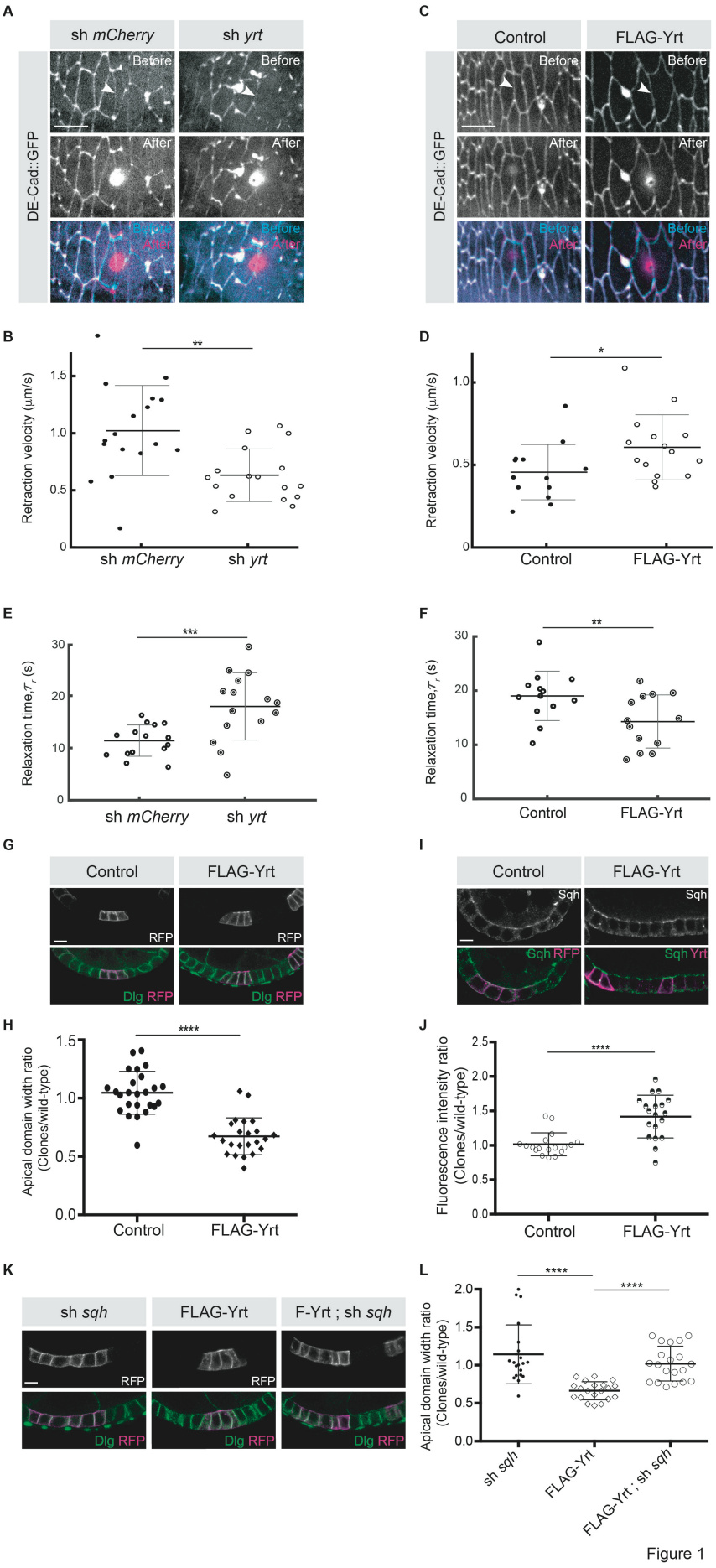
A
sh mCherry
sh yrt
DE-Cad::GFP
Before
After
C
Control
FLAG-Yrt
B
Retraction velocity (μm/s)
sh mCherry
sh yrt
D
Rretraction velocity (μm/s)
Control
FLAG-Yrt
E
Relaxation time,τr (s)
F
G
RFP
Dlg RFP
I
Sqh
Sqh RFP
Sqh Yrt
H
Apical domain width ratio (Clones/wild-type)
J
Fluorescence intensity ratio (Clones/wild-type)
K
sh sqh
F-Yrt ; sh sqh
L

Figure 1

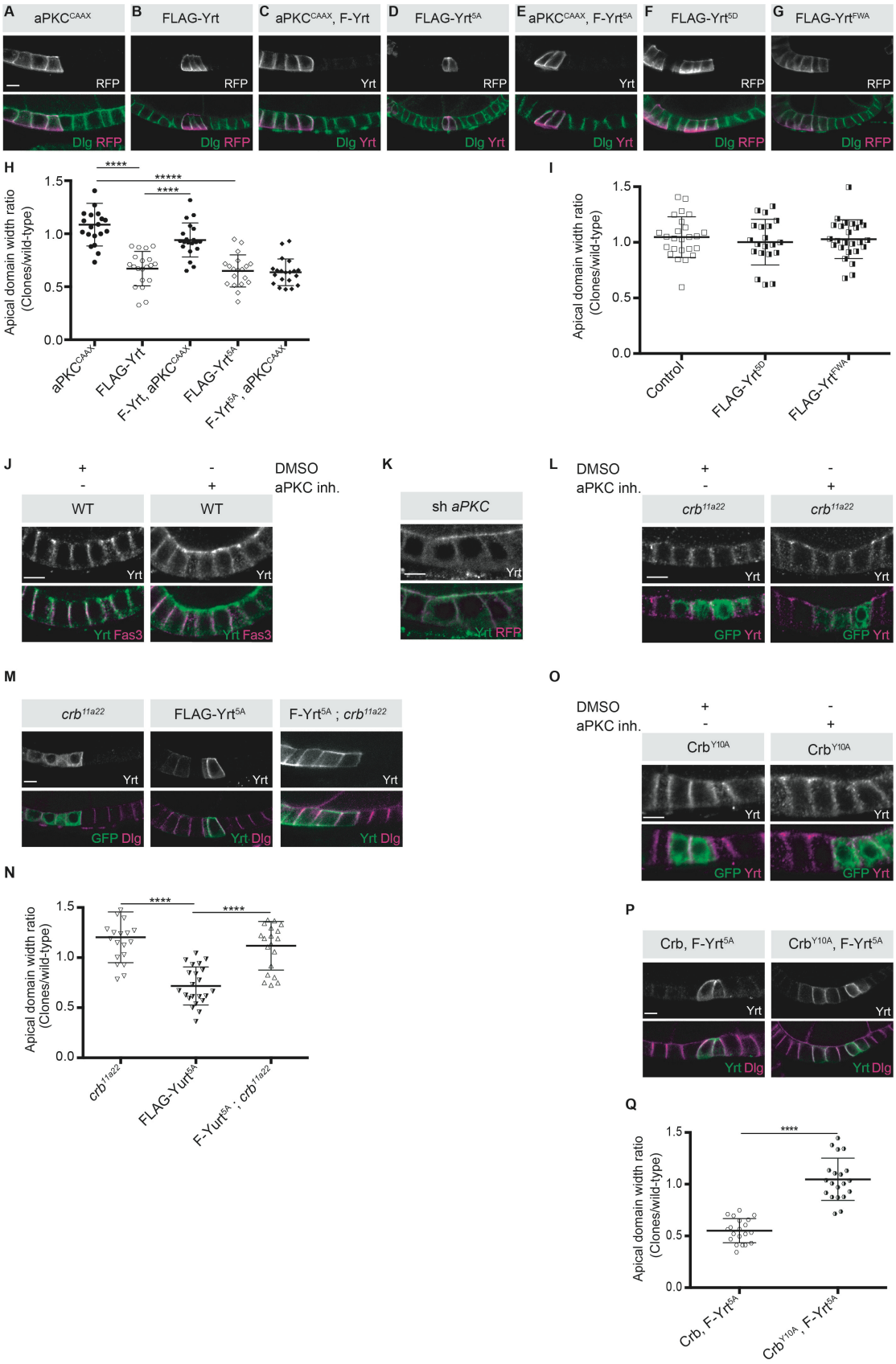
A aPKC^CAAX
B FLAG-Yrt
C aPKC^CAAX, F-Yrt
D FLAG-Yrt^5A
E aPKC^CAAX, F-Yrt^5A
F FLAG-Yrt^5D
G FLAG-Yrt^FWA
RFP
Yrt
Dlg RFP
Dlg Yrt
H
Apical domain width ratio (Clones/wild-type)
aPKC^CAAX
FLAG-Yrt
F-Yrt, aPKC^CAAX
FLAG-Yrt^5A
F-Yrt^5A, aPKC^CAAX
I
Control
FLAG-Yrt^5D
FLAG-Yrt^FWA
J
DMSO
aPKC inh.
WT
Yrt Fas3
K
sh aPKC
Yrt RFP
L
crb^11a22
GFP Yrt
M
FLAG-Yrt^5A
F-Yrt^5A ; crb^11a22
GFP Dlg
Yrt Dlg
N
O
Crb^Y10A
P
Crb, F-Yrt^5A
Crb^Y10A, F-Yrt^5A
Q

Figure 2

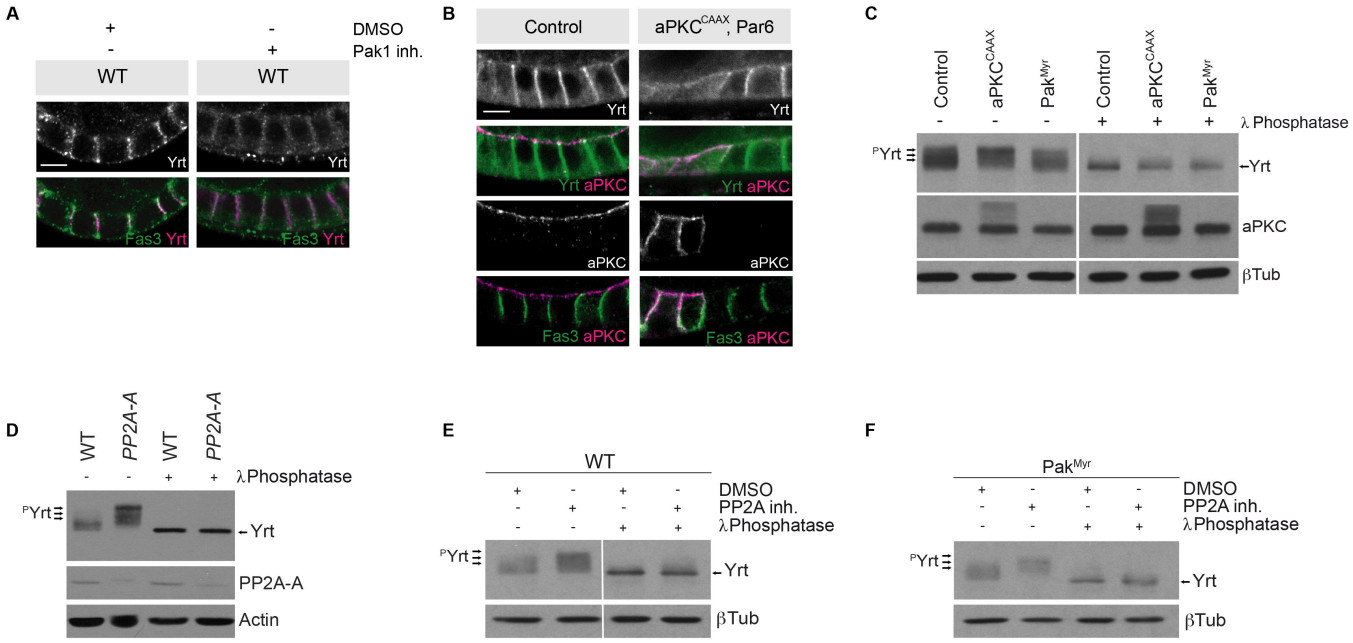
A
+
-
DMSO
-
+
Pak1 inh.
WT
WT
Yrt
Yrt
Fas3 Yrt
Fas3 Yrt
B
Control
aPKC^CAAX; Par6
Yrt
Yrt
Yrt aPKC
Yrt aPKC
aPKC
aPKC
Fas3 aPKC
Fas3 aPKC
C
Control
aPKC^CAAX
Pak^Myr
Control
aPKC^CAAX
Pak^Myr
- - - + + + λ Phosphatase
^PYrt
Yrt
aPKC
βTub
D
WT
PP2A-A
WT
PP2A-A
- - + + λPhosphatase
^PYrt
Yrt
PP2A-A
Actin
E
WT
+ - + - DMSO
- + - + PP2A inh.
- - + + λPhosphatase
^PYrt
Yrt
βTub
F
Pak^Myr
+ - + - DMSO
- + - + PP2A inh.
- - + + λPhosphatase
^PYrt
Yrt
βTub

Figure 3

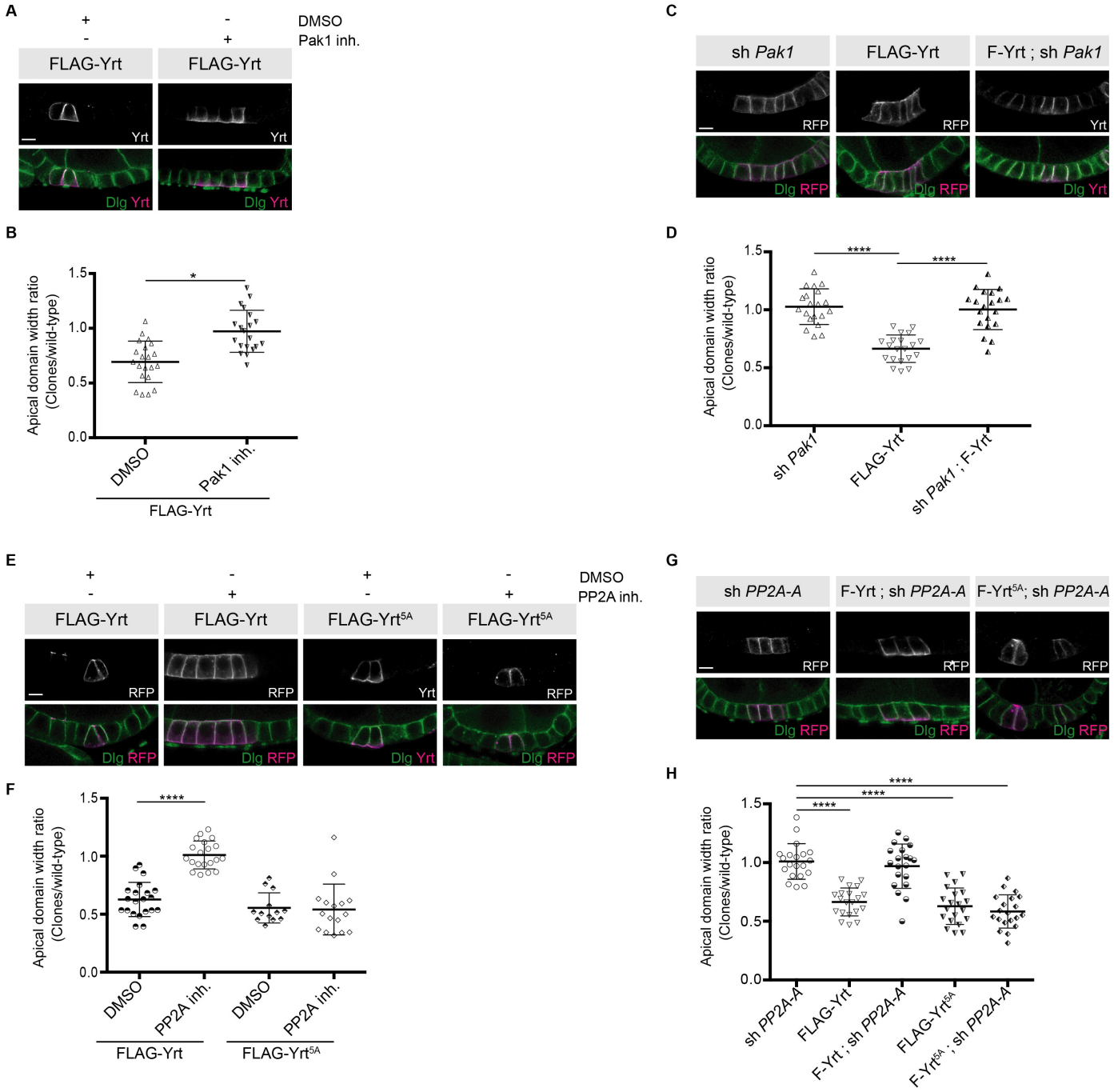
A
+
-
DMSO
-
+
Pak1 inh.
FLAG-Yrt
FLAG-Yrt
Yrt
Yrt
Dlg Yrt
Dlg Yrt
B
Apical domain width ratio (Clones/wild-type)
1.5
1.0
0.5
0.0
*
DMSO
Pak1 inh.
FLAG-Yrt
C
sh Pak1
FLAG-Yrt
F-Yrt ; sh Pak1
RFP
RFP
Yrt
Dlg RFP
Dlg RFP
Dlg Yrt
D
Apical domain width ratio (Clones/wild-type)
1.5
1.0
0.5
0.0
****
****
sh Pak1
FLAG-Yrt
sh Pak1 ; F-Yrt
E
+
-
+
-
DMSO
-
+
-
+
PP2A inh.
FLAG-Yrt
FLAG-Yrt
FLAG-Yrt5A
FLAG-Yrt5A
RFP
RFP
Yrt
RFP
Dlg RFP
Dlg RFP
Dlg Yrt
Dlg RFP
F
Apical domain width ratio (Clones/wild-type)
1.5
1.0
0.5
0.0
****
DMSO
PP2A inh.
DMSO
PP2A inh.
FLAG-Yrt
FLAG-Yrt5A
G
sh PP2A-A
F-Yrt ; sh PP2A-A
F-Yrt5A; sh PP2A-A
RFP
RFP
RFP
Dlg RFP
Dlg RFP
Dlg RFP
H
Apical domain width ratio (Clones/wild-type)
1.5
1.0
0.5
0.0
****
****
****
sh PP2A-A
FLAG-Yrt
F-Yrt ; sh PP2A-A
FLAG-Yrt5A
F-Yrt5A ; sh PP2A-A

Figure 4

Table 1 : List of fly stocks used in this study

Genotype	**Source**	**Identifier**
D. melanogaster: UAS-FLAG-Yurt	Reference (20)	N/A
D. melanogaster: UAS-FLAG-Yurt[5A]	Reference (20)	N/A
D. melanogaster: UAS-FLAG-Yurt[FWA]	Reference (54)	N/A
D. melanogaster: UAS-FLAG-Yurt[5D]	Reference (20)	N/A
D. melanogaster: UAS-sh yurt	Drosophila Bloomington Stock Centre	# 36118
D. melanogaster: UAS-sh squash	Drosophila Bloomington Stock Centre	# 32439
D. melanogaster: UAS-aPKC[CAAX]	Reference (66)	N/A
D. melanogaster: UAS-aPKC[CAAX], Par6	Gift from T. Harris (David et al., 2010)	N/A
D. melanogaster: UAS-sh mCherry	Drosophila Bloomington Stock Centre	# 35785
D. melanogaster: FRT82b, crb[11a22]	Drosophila Bloomington Stock Centre	# 3448
D. melanogaster: UAS-sh aPKC	Drosophila Bloomington Stock Centre	# 34332
D. melanogaster: UAS-sh Pak1	Drosophila Bloomington Stock Centre	# 41714
D. melanogaster: UAS-Pak[myr]	Drosophila Bloomington Stock Centre	# 8804
D. melanogaster: foscrb[Y10A] ; FRT82b, crb[11a22]	Reference (10)	N/A
D. melanogaster: UAS-LacZ	Drosophila Bloomington Stock Centre	# 8529
D. melanogaster: sh Pp2a-A	Drosophila Bloomington Stock Centre	# 55050
D. melanogaster: endo-E-Cadherin::GFP	Reference (82)	N/A
D. melanogaster: sqh-sqh::GFP	Reference (83)	N/A
D. melanogaster: matαtub67;15-GAL4	Reference (84)	N/A
D. melanogaster: daughterless-GAL4	Drosophila Bloomington Stock Centre	# 27608
D. melanogaster: hs-FLP;; tub-FRT-Gal80-FRT-Gal4, UAS–mRFP	Gift from Y. Bellaiche, Institut Curie, PSL Research University, Paris, France.	N/A
D. melanogaster: hs-FLP; tub-GAL4, UAS-GFP; FRT82b, tub-GAL80	Gift from N. Perrimon, Harvard Medical School, Boston, USA	N/A

D. melanogaster: hs-FLP; sqh-Sqh::GFP; tub>Gal80>Gal4, UAS–mRFP	Gift from Y. Bellaiche, Institut Curie, PSL Research University, Paris, France.	N/A
D. melanogaster: wild type	Drosophila Bloomington Stock Centre	# 25210
D. melanogaster: PP2A-A[EP2332] / Cyo	Drosophila Bloomington Stock Centre	# 1704

Table 2 : List of detailed genotypes in each figure

Figure 1

A *mat-GAL4 / endo-E-Cadherin::GFP ; UAS-sh mCherry / matαtub67;15-GAL4*

mat-GAL4 / endo-E-Cadherin::GFP ; UAS-sh yrt / matαtub67;15-GAL4

B *mat-GAL4 / endo-E-Cadherin::GFP ; UAS-sh mCherry / matαtub67;15-GAL4*

mat-GAL4 / endo-E-Cadherin::GFP ; UAS-sh yrt / matαtub67;15-GAL4

C *endo-E-Cadherin::GFP ; daughterless-GAL4*

endo-E-Cadherin::GFP ; UAS-FLAG-Yrt / daughterless-GAL4

D *endo-E-Cadherin::GFP ; daughterless-GAL4*

endo-E-Cadherin::GFP ; UAS-FLAG-Yrt / daughterless-GAL4

E *hs-FLP / + ;; UAS- LacZ / tub-FRT-GAL80-FRT-GAL4, UAS–mRFP*

hs-FLP / + ;; UAS- FLAG-Yrt / tub-FRT-GAL80-FRT-GAL4, UAS–mRFP

F *hs-FLP / + ;; UAS- LacZ / tub-FRT-GAL80-FRT-GAL4, UAS–mRFP*

hs-FLP / + ;; UAS- FLAG-Yrt / tub-FRT-GAL80-FRT-GAL4, UAS–mRFP

G *hs-FLP; sqh-Sqh::GFP; UAS-LacZ / tub-FRT-GAL80-FRT-GAL4, UAS–mRFP*

hs-FLP; sqh-Sqh::GFP; UAS-FLAG-Yrt / tub-FRT-GAL80-FRT-GAL4, UAS–mRFP

H *hs-FLP; sqh-Sqh::GFP; UAS-LacZ / tub-FRT-GAL80-FRT-GAL4, UAS–mRFP*

hs-FLP; sqh-Sqh::GFP; UAS-FLAG-Yrt / tub-FRT-GAL80-FRT-GAL4, UAS–mRFP

Figure 2

A *hs-FLP / + ;; UAS- aPKC[CAAX] / tub-FRT-GAL80-FRT-GAL4, UAS–mRFP*

B *hs-FLP / + ; UAS- LacZ ; UAS- FLAG-Yrt / tub-FRT-GAL80-FRT-GAL4, UAS–mRFP*

C *hs-FLP / + ;; UAS-aPKC[CAAX], UAS- FLAG-Yrt / tub-FRT-GAL80-FRT-GAL4, UAS–mRFP*

D *hs-FLP / + ; UAS- LacZ ; UAS- FLAG-Yrt[5A] / tub-FRT-GAL80-FRT-GAL4, UAS–mRFP*

E *hs-FLP / + ;; UAS-aPKC[CAAX], UAS- FLAG-Yrt[5A] / tub-FRT-GAL80-FRT-GAL4, UAS–mRFP*

F *hs-FLP / + ;; UAS- FLAG-Yrt[5D] / tub-FRT-GAL80-FRT-Gal4, UAS–mRFP*

G *hs-FLP / + ;; UAS- FLAG-Yrt[FWA] / tub-FRT-GAL80-FRT-Gal4, UAS–mRFP*

H *hs-FLP / + ;; UAS- aPKC[CAAX] / tub-FRT-GAL80-FRT-GAL4, UAS–mRFP*

hs-FLP / + ; UAS- LacZ ; UAS- FLAG-Yrt / tub-FRT-GAL80-FRT-GAL4, UAS–mRFP

hs-FLP / + ;; UAS-aPKC[CAAX], UAS- FLAG-Yrt / tub-FRT-GAL80-FRT-GAL4, UAS–mRFP

hs-FLP / + ; UAS- LacZ ; UAS- FLAG-Yrt[5A] / tub-FRT-GAL80-FRT-GAL4, UAS–mRFP

hs-FLP / + ;; UAS-aPKC[CAAX], UAS- FLAG-Yrt[5A] / tub-FRT-GAL80-FRT-GAL4, UAS–mRFP

I *hs-FLP / + ; UAS- LacZ ; + / tub-FRT-GAL80-FRT-GAL4, UAS–mRFP*

hs-FLP / + ;; UAS- FLAG-Yrt[5A] / tub-FRT-GAL80-FRT-Gal4, UAS–mRFP

hs-FLP / + ;; UAS- FLAG-Yrt[5D] / tub-FRT-GAL80-FRT-Gal4, UAS–mRFP

hs-FLP / + ;; UAS- FLAG-Yrt[FWA] / tub-FRT-GAL80-FRT-Gal4, UAS–mRFP

J *wild type* ovaries treated with DMSO or aPKC inhibitor

K *hs-FLP / + ;; sh aPKC / tub-FRT-GAL80-FRT-GAL4, UAS–mRFP*

L *hs-FLP; tub-GAL4, UAS-GFP / + ; FRT82b, crb[11a22] / FRT82b,tub-GAL80* treated with DMSO or aPKC inhibitor

M *hs-FLP; tub-GAL4, UAS-GFP / UAS-LacZ ; FRT82b, crb[11a22] / FRT82b,tub-GAL80*

hs-FLP; tub-GAL4, UAS-GFP / UAS-FLAG-Yrt[5A] ; FRT82b / FRT82b,tub-GAL81

hs-FLP; tub-GAL4, UAS-GFP / UAS-FLAG-Yrt[5A] ; FRT82b, crb[11a22] / FRT82b,tub-GAL80

N *hs-FLP; tub-GAL4, UAS-GFP / UAS-LacZ ; FRT82b, crb[11a22] / FRT82b,tub-GAL80*

hs-FLP; tub-GAL4, UAS-GFP / UAS-FLAG-Yrt[5A] ; FRT82b / FRT82b,tub-GAL81

hs-FLP; tub-GAL4, UAS-GFP / UAS-FLAG-Yrt[5A] ; FRT82b, crb[11a22] / FRT82b,tub-GAL80

O *hs-FLP; tub-GAL4, UAS-GFP / fosCrb[Y10A] ; FRT82b, crb[11a22] / FRT82b,tub-GAL80* treated with DMSO or aPKC inhibitor

P *hs-FLP; tub-GAL4, UAS-GFP / fosCrb[Y10A] ; FRT82b, crb[11a22] / FRT82b,tub-GAL80*

hs-FLP; tub-GAL4, UAS-GFP / UAS-FLAG-Yrt[5A], fosCrb[Y10A] ; FRT82b, crb[11a22] / FRT82b,tub-GAL80

Q *hs-FLP; tub-GAL4, UAS-GFP / fosCrb[Y10A] ; FRT82b, crb[11a22] / FRT82b,tub-GAL80*

Figure 3

A *wild type* ovaries treated with DMSO or Pak1 inhibitor

B *hs-FLP / + ;; UAS- LacZ / tub-FRT-Gal80-FRT-Gal4, UAS–mRFP*

hs-FLP / + ;; UAS-aPKC[CAAX], Par6 / tub-FRT-GAL80-FRT-GAL4, UAS–mRFP

C *Daughterless-GAL4 / + ; UAS-FLAG-GFP / Daughterless-GAL4*

Daughterless-GAL4 / + ; UAS-aPKC[CAAX], Par6 / Daughterless-GAL4

Daughterless-GAL4 / + ; UAS-Pak[myr] / Daughterless-GAL4

D *wild type*

Pp2A-29b[EP2332]

E *wild type embryos treated with DMSO or PP2A inhibitor*

Figure 4

A *hs-FLP / + ;; UAS- FLAG-Yrt / tub-FRT-GAL80-FRT-GAL4, UAS–mRFP* treated with DMSO or Pak1 inhibitor

B *hs-FLP / + ;; UAS- FLAG-Yrt / tub-FRT-GAL80-FRT-GAL4, UAS–mRFP* treated with DMSO or Pak1 inhibitor

C *hs-FLP / + ; sh lexA ; + / tub-FRT-GAL80-FRT-GAL4, UAS–mRFP*

hs-FLP / + ; sh lexA ; UAS- FLAG-Yrt / tub-FRT-GAL80-FRT-GAL4, UAS–mRFP

hs-FLP / + ; sh Pak ; UAS- FLAG-Yrt / tub-FRT-GAL80-FRT-GAL4, UAS–mRFP

D *hs-FLP / + ; sh lexA ; + / tub-FRT-GAL80-FRT-GAL4, UAS–mRFP*

hs-FLP / + ; sh lexA ; UAS- FLAG-Yrt / tub-FRT-GAL80-FRT-GAL4, UAS–mRFP

hs-FLP / + ; sh Pak ; UAS- FLAG-Yrt / tub-FRT-GAL80-FRT-GAL4, UAS–mRFP

E *hs-FLP / + ;; UAS- FLAG-Yrt / tub-FRT-GAL80-FRT-GAL4, UAS–mRFP* treated with DMSO or PP2A inhibitor

hs-FLP / + ;; UAS- FLAG-Yrt[5A] / tub-FRT-GAL80-FRT-GAL4, UAS–mRFP treated with DMSO or PP2A inhibitor

F *hs-FLP / + ;; UAS- FLAG-Yrt / tub-FRT-GAL80-FRT-GAL4, UAS–mRFP* treated with DMSO or PP2A inhibitor

hs-FLP / + ;; UAS- FLAG-Yrt[5A] / tub-FRT-GAL80-FRT-GAL4, UAS–mRFP treated with DMSO or PP2A inhibitor

G *hs-FLP / + ;; sh Pp2A-29b / tub-FRT-GAL80-FRT-GAL4, UAS–mRFP*

hs-FLP / + ; UAS-FLAG-Yrt ; sh Pp2A-29b / tub-FRT-GAL80-FRT-GAL4, UAS–mRFP

hs-FLP / + ; UAS-FLAG-Yrt[5A] ; sh Pp2A-29b / tub-FRT-GAL80-FRT-GAL4, UAS–mRFP

H *hs-FLP / + ;; sh Pp2A-29b / tub-FRT-GAL80-FRT-GAL4, UAS–mRFP*

hs-FLP / + ; UAS-FLAG-Yrt ; sh Pp2A-29b / tub-FRT-GAL80-FRT-GAL4, UAS–mRFP

hs-FLP / + ; UAS-FLAG-Yrt[5A] ; sh Pp2A-29b / tub-FRT-GAL80-FRT-GAL4, UAS–mRFP